RSC Advances

Nanoflaky MnO2 grown in situ on carbon microbead as anode materials for high-performance lithium-ion batteries

Journal:	*RSC Advances*
Manuscript ID:	RA-COM-03-2014-001922.R2
Article Type:	Communication
Date Submitted by the Author:	02-May-2014

Complete List of Authors:	Wang, Hao; Xiangtan University, School of Chemistry Liu, Jing; Xiangtan University, School of Chemistry wang, xianyou; Xiangtan University, shool of chemistry Wu, Chun; Xiangtan University, School of Chemistry Zhao, Qinglan; Xiangtan University, School of Chemistry Fu, Yanqing; Xiangtan University, School of Chemistry yang, xiukang; Xiangtan University, School of Chemistry Shu, Hongbo; Xiangtan University, School of Chemistry

Nanoflaky MnO_2 grown *in situ* on carbon microbead as anode materials for high-performance lithium-ion batteries

Hao Wang, Jing Liu, Xianyou Wang*, Chun Wu, Qinglan Zhao, Yanqing Fu, Xiukang Yang, Hongbo Shu*

Key Laboratory of Environmentally Friendly Chemistry and Applications of Ministry of Education, School of Chemistry, Xiangtan University, Hunan, Xiangtan 411105, China

Abstract: Flower-like MnO_2 encapsulated carbon microbead (MnO_2@CMB) nanocomposite is firstly synthesized via an *in situ* nucleation and growth of birnessite-type MnO_2 on the surface of monodisperse carbon microbead. The structure, morphology and performance of the samples are characterized by powder X-ray diffraction (XRD), scanning electron microscopy (SEM), and galvanostatic charge/discharge. The results reveal that the flower texture MnO_2@CMB nanocomposite is composed of CMB core and nanosheet MnO_2 shell. As the anode material for lithium-ion batteries, the MnO_2@CMB nanocomposite exhibits excellent electrochemical performances. It shows a good rate capability of 230 mAh g^{-1} at the current density of 1500 mA g^{-1} and a large reversible capacity of 620 mAh g^{-1} without capacity fade for the 80^{th} cycles at 100 mA g^{-1}, which is much better than those of pure MnO_2 and graphite. The superior electrochemical performance can be attributed to the unique hierarchical architecture and the combinative effects of the nanosheet MnO_2 and carbon matrices.

***Keywords*:** Lithium-ion batteries; Composite materials; Manganese oxide; Carbon microbeads; Anode

* **Corresponding author:** Xianyou Wang Tel: +86 731 58292060; fax: +86 731 58292061.
E-mail address: wxianyou@yahoo.com (X. Wang).

* **Corresponding author:** hongboshuxtu@gmail.com

1. Introduction

Recently, some transition metal oxides (TMOs) have been considered to be promising anode materials for LIBs owing to their high theoretical capacity and low cost [1, 2]. Among all of the TMOs, MnO_2 has attracted great attention due to its natural abundance, environmental friendliness and low cost [3]. As an anode material, MnO_2 has many advantages compared with currently commercially used graphite, such as its relatively high theoretical capacity (about 755 mAh g^{-1}) and low overpotential [4]. Therefore, the MnO_2 samples with various crystallographic structure (such as α, β, γ, and δ) and morphology (including rods, wires, tubes, and urchin-like microstructures) have been synthesized [5]. However, there still exist many challenges in the applications of MnO_2-based electrodes, such as the less reversible capacity and faster capacity fade [6]. Usually, these problems can be attributed to its poor electronic conductivity, low ion diffusion constant, large volume expansion and others. Extensive researches have been done to solve these problems. Among these studies, the MnO_2/C nanocomposite is considered to be one of the most realistic approaches, such as MnO_2/C core-shell nanorodes [7], coaxial MnO_2/C nanotubes [8] and MnO_2/C hybrids [9]. Although many composites have been designed and studied, most of these studies focused on the method, in which the surface of MnO_2 is covered with electrically conductive carbon layers. These materials still suffer from electrochemical stability problems

In this paper, a facile hydrothermal method has been designed to synthesize flower texture MnO_2@CMB with the MnO_2 shell and the CMB core. As $KMnO_4$ is reduced by carbon in CMB, the resultant MnO_2 is *in situ* nucleating on the surface of

CMB, and then the MnO_2@CMB nanocomposite is formed via a hydrothermal process. The obtained MnO_2@CMB is explored as the anode for LIBs, and the electrochemical performances are investigated in details.

2. Experimental

2.1. Sample synthesis

All the reagents were of analytical grade and used without further purification. The CMB was prepared by a hydrothermal method reported in our previous literature and activated in 16 M HNO_3 solution at 70 ^oC for 24 h[10]. For comparison, pure MnO_2 nanoparticles were also prepared as in Ref. [11].

A simple process of the synthesis of flower texture MnO_2@CMB nanocomposite is described as follows: designed amount CMB and $KMnO_4$ were mixed in 75 ml deionized water, followed by stirring for 1 h. Then the mixture were transferred into a Teflon-lined autoclave (100 ml), sealed and put in an electric oven at 160 ^oC for 10 h. After the mixtures were naturally cooled to room temperature, the precipitation was filtered and washed with distilled water. Finally, the MnO_2@CMB samples were dried at 80 ^oC for 10 h in the air and dried further in order to remove crystal water. The analysis for composition of MnO_2@CMB nanocomposite was carried out by means of atomic absorption spectroscopy (AAS) and TGA measurement.

2.2. Physical and electrochemical measurements

Morphology of sample was characterized by scanning electron microscopy (SEM) (Hitachi S-3500N). The morphology and structure of the MnO_2@CMB were further investigated by transmission electron microscopy (TEM) (JEM-2100F, JEOL). The

crystallographic analyses of samples were carried out by X-ray diffraction (XRD) (D/max-2550 Rigaku, Japan). The contents of CMB in the nanocomposite were determined by thermogravimetric analysis (TGA) (WRT-3P, Shanghai China).

The electrodes were prepared by the mixed slurry containing active materials (75 wt%), acetylene black (15 wt%) and polyvinylidene fluoride (PVDF 10 wt%) in N-methyl-2-pyrrolidone (NMP). The slurry was pasted on the Cu foil and dried for 12 h at 110 ^{o}C in the vacuum. The electrolyte was consisted of 1 M $LiPF_6$ in ethylene carbonate (EC) and dimethyl carbonate (DMC) (1:1, V/V). Half cells using pure Li foil as both counter and reference electrodes were assembled by a 2025 coin-type cell. Charge/discharge measurement was carried out in Neware battery test system BTS-XWJ-6.44S-00052 (Newell, China). The electrochemical impedance spectroscopys (EIS) of the cells were measured on a VersaSTAT3 electrochemical workstation (Princeton, America) in the frequency range of 10 kHz to 10 mHz with an AC voltage of 5 mV.

3. Results and discussion

Fig. 1(a-d) exhibits the morphology of the CMB, pure MnO_2 and MnO_2@CMB nanocomposite. It has been known from chemical analysis that the MnO_2@CMB nanocomposite is composed of 9 wt.% CMB and 91 wt.% MnO_2. As shown in Fig. 1a and b, CMB shows a good sphericity and a smooth surface, and the pure MnO_2 exhibit a flower texture. The microstructure of MnO_2@CMB nanocomposite is showed in Fig. 1c. The flower texture MnO_2 layer with highly porous structure is uniformly deposited on the surface of CMB. By comparing Fig. 1b with c, it is found

that the MnO_2@CMB nanocomposite is very similar to pure MnO_2 in morphology. A fragment of bulky MnO_2@CMB nanocomposite was selected and displayed in Fig. 1d to observe the internal structure of MnO_2@CMB nanocomposite clearly and demonstrate its formation mechanism. The bulky CMB fragment is surrounded by the nanosheet MnO_2 with the drawn white curve as a rough separation. Within the white curve it is the bulky CMB fragment, and the appearance is the nanosheet MnO_2. It is evident that as the MnO_2 is growing on the CMB, the CMB surface is slightly corroded. The detailed morphology of MnO_2@CMB nanocomposite can be further confirmed by TEM (Fig. 1e) and HRTEM (Fig. 1f). It can be observed from TEM image in Fig. 1e that CMB is covered uniformly by a thick layer of MnO_2 nanosheet with a good morphology. Besides, the size of the CMB in the nanocomposite is slightly less than the one of the original CMB. This can probably be attributed to the corrosion of CMB in the process of formation of MnO_2 nanosheet. The interplanar spacing of MnO_2 nanoflake measured from the HRTEM image is 0.68 nm on average, which is in good agreement with approximately 0.7 nm reported in the literature for birnessite-type MnO_2 [12].

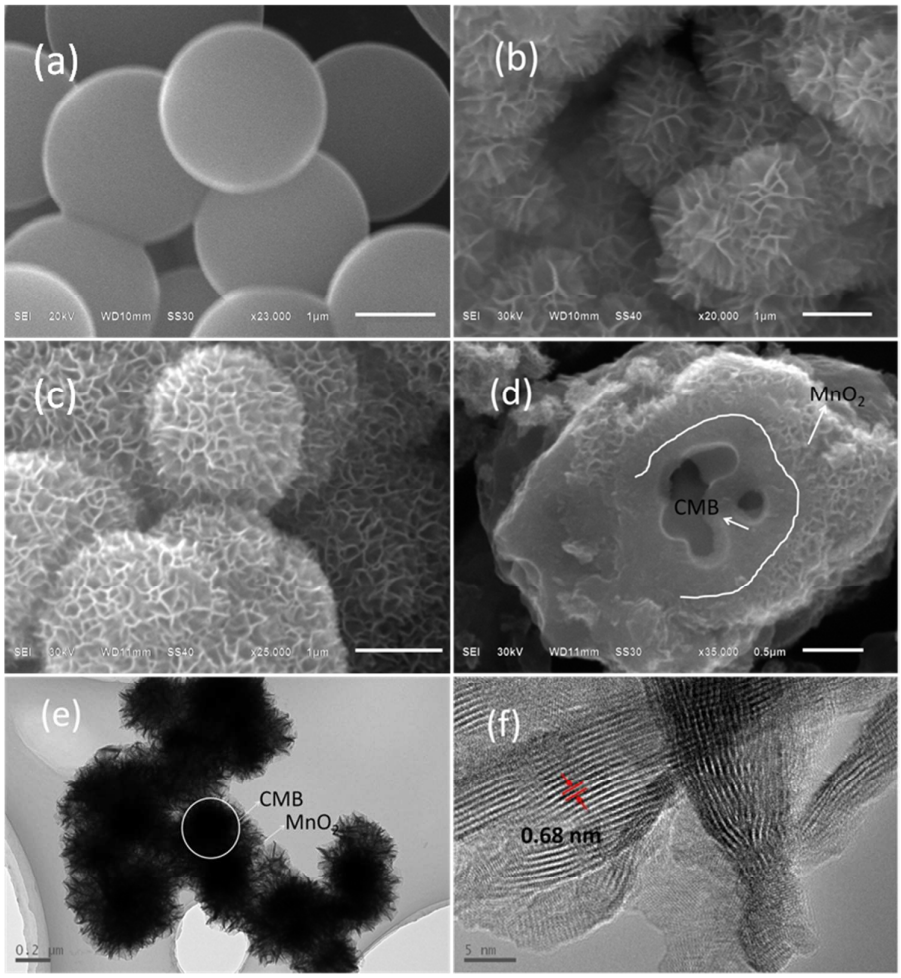

Fig. 1 SEM images of (a) the pristine CMB, (b) the pure MnO_2 nanosheet, (c) the flower texture MnO_2@CMB, (d) the fragment of bulky MnO_2@CMB; (e) TEM image of the CMB coated with MnO_2 nanosheet; (f) HRTEM image of the MnO_2 nanosheet grown on the surface of CMB

The XRD patterns of the as-prepared CMB, pure MnO_2 and MnO_2@CMB nanocomposite are showed in Fig. 2a. There are two broad diffraction peaks positioned at around 23° and 43° in the XRD pattern of CMB, which correspond to the diffraction bands (002) and (100/101) of graphite respectively [13]. Besides, all the marked peaks of pure MnO_2 can be indexed to the monoclinic potassium birnessite (JCPDS 80-1098) that consists of 2D, edge-shared MnO_6 octahedral layers with K^+ cations and water molecules in the interlayer space [14]. Moreover, the XRD pattern of

flower texture MnO_2@CMB nanocomposite has all the characteristic peaks of pure MnO_2 phase without any impurities. The contents of CMB in MnO_2@CMB nanocomposite were evaluated by TGA measurement, as shown in Fig. 2b. The 9% weight loss is ascribed to the oxidation of the CMB between 450-550 ^oC in air. Therefore, the content of CMB in flower texture MnO_2@CMB nanocomposite is about 9%.

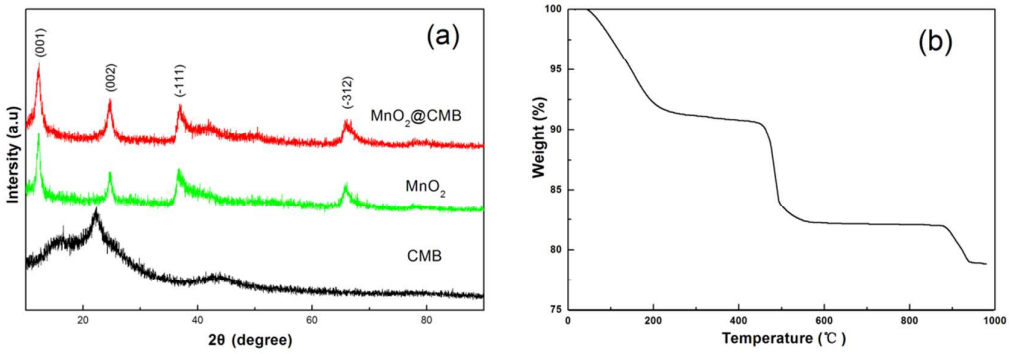

Fig. 2 (a) XRD patterns of CMB, pure MnO_2 and MnO_2@CMB; (b) TGA curve of the MnO_2@CMB.

As for the growth mechanism of the MnO_2@CMB, it is considered that the CMB is first dispersed in the $KMnO_4$ solution, then the mixed solution undergoes a hydrothermal process, Mn^{7+} is reduced into Mn^{4+}, finally the flower texture MnO_2 is formed on the surface of CMB. At the beginning, the nanocrystalline MnO_2 is formed on the surface of the CMB through the redox process given by Eq (1) [15], which promotes the decomposition of $KMnO_4$ given by Eq (2) [16]. However, the CMB is eroded obviously as detected from Fig. 1d, which indicates that the redox process still exists in the consequent reaction along with the decomposition of $KMnO_4$. With the MnO_2 growing on the surface of CMB, the contacted surface of CMB with $KMnO_4$ solution decreases. Then, the formation of MnO_2 through decomposition of $KMnO_4$

can be dominant in the following hydrothermal process. Consequently, the flower texture MnO_2@CMB nanocomposite is easily formed via this simple hydrothermal method.

(1)

(2)

The electrochemical performances of the as-prepared flower texture MnO_2@CMB nanocomposite and flower texture pure MnO_2 as anode material were investigated by galvanostatic charge/discharge measurement. Fig. 3(a, b) show that the representative voltage profiles of the 1^{st}, 2^{th}, 10^{th} and 50^{th} cycles for the MnO_2@CMB nanocomposite and the pure MnO_2 electrodes, which are cycled between 0.01V and 3 V at a current density of 100 mA g^{-1}. The first discharge and charge capacity of MnO_2@CMB nanocomposite are 1480 mAh g^{-1} and 698 mAh g^{-1}, respectively, whereas in the case of the pure MnO_2 anode the first discharge and charge capacity are 1210 mAh g^{-1} and 523 mAh g^{-1}, respectively. The large irreversible capacity can be mainly attributed to the formation of a solid electrolyte interface film on the surface of the electrode materials [17]. Besides, it can be seen that the MnO_2@CMB electrode exhibits a much smaller irreversible capacity than the pure MnO_2 electrode after the first cycle. Fig. 3c shows that the comparison of the cyclic performance of

the MnO_2@CMB electrode with that of the pure MnO_2 electrode, cycled between 0.01V and 3V at the current density of 100 mA g^{-1} for 100 cycles. Moreover, for the pure MnO_2 electrode, the reversible capacity continuously decays as the cyclic number increases before 20 cycles, after 40 cycles the capacity fades fast, and its capacity only remains 205 mAh g^{-1} after 100 cycles. The pure CMB exhibits the discharge capacity of about 100 mAh g^{-1} after 100 cycles. However, the MnO_2@CMB electrode exhibits a reversible capacity of around 620 mAh g^{-1} until 80 cycles and retains 525 mAh g^{-1} after 100 cycles.

In order to discuss the effect of the composition on the performance of MnO_2@CMB nanocomposite, the rate performances of the MnO_2@CMB nanocomposites with different CMB contents (MnO_2@CMB1 is about 9 wt.% CMB, and MnO_2@CMB2 is about 15 wt.% CMB) and pure MnO_2 electrodes were evaluated at different current densities, as shown in Fig. 3d. With the current density increasing, the discharge capacity remains 640-700, 530-550, 360-390, 280-290, 225-230 mAh g^{-1} at the current densities of 100, 200, 500, 1000, 1500 mA g^{-1}, respectively. When the current is returned to 100 mA g^{-1}, the MnO_2@CMB electrode returns its initial capacity, indicating that the excellent rate performance of MnO_2@CMB anode is better than those of the pure MnO_2. Moreover, with the increase of the CMB the rate performance of the nanocomposite will be improved, but the discharge capacity will be slightly reduced.

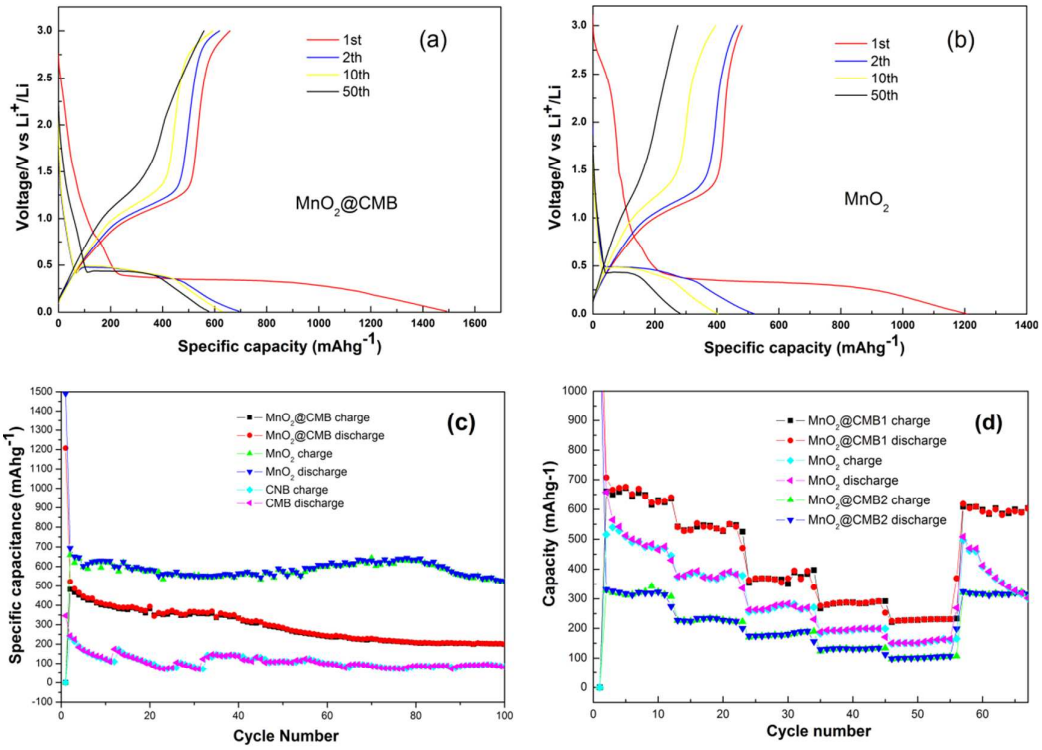

Fig. 3 Typical discharge/charge voltage profiles of (a) MnO_2@CMB and (b) pure MnO_2 at a current density of 100 mA g^{-1}; (c) Comparative cycling performance of MnO_2@CMB pure MnO_2 and CMB at a current density of 100 mA g^{-1}; (d) Comparison of rate capability of MnO_2@CMB with different CMB contents (9 wt.%, 15wt.%) and pure MnO_2.

Electrochemical impedance spectroscopy (EIS) was carried out to measure the MnO_2@CMB reaction resistance. The Nyquist plots of MnO_2@CMB and pure MnO_2 are shown in Fig.4. The both Nyquist plots show the similar shape, they are consisted of a semicircle at the high frequency and an inclined line following at the low frequency, which corresponds to the charge-transfer resistance at the electrode/electrolyte interface and the lithium ion-diffusion process within electrodes. Obviously, it can be found that the reaction resistance of MnO_2@CMB is much less than that of pure MnO_2.

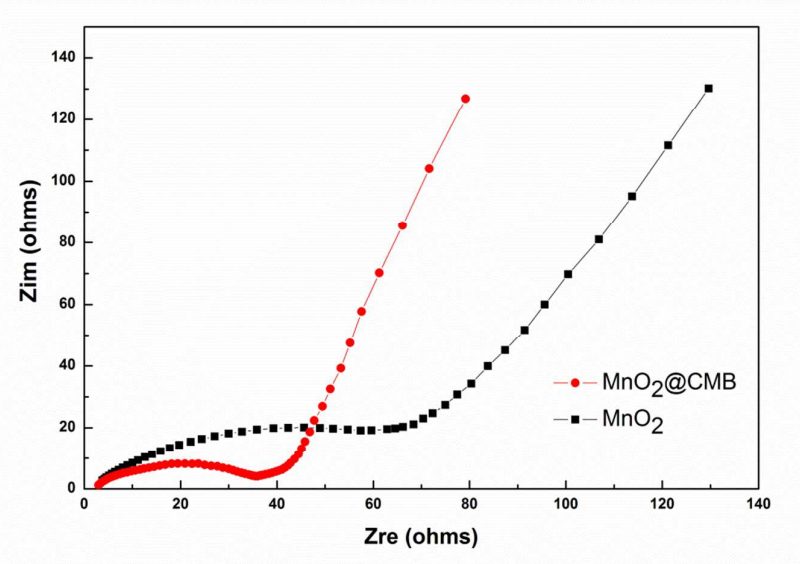

Fig. 4 Nyquist plots for MnO_2@CMB and pure MnO_2.

4. Conclusions

By using CMB as the carbon precursor, the flower texture MnO_2@CMB nanocomposite with a CMB core and nanosheet MnO_2 shell has been synthesized. As the anode material for LIBs, the MnO_2@CMB nanocomposite exhibits a high reversible capacity, good cycle performance and excellent rate capability. Compared to that of pure MnO_2 with similar morphology, higher lithium storage performance of the MnO_2@CMB nanocomposite can be attributed to its novel hierarchical architecture that can enhance ion and electron transport. Therefore, the MnO_2@CMB nanocomposite could be a promising electrode material for LIBs and other applications such as catalysis and supercapacitors.

Acknowledgements

This work is funded by the National Natural Science Foundation of China under project No. 51272221, Scientific and Technical Achievement Transformation Fund of Hunan Province under project No. 2012CK1006, Key Project of Strategic New Industry of Hunan Province under project No. 2013GK4018, and Science and

Technology plan Foundation of Hunan Province under project no. 2013FJ4062.

References

1 C.X. Zu, H. Li, Energy Environ. Sci. 2011, 4, 2614.

2 J. Xie, W. Song, G. Cao, T. Zhu, X. Zhao, S. Zhang, RSC Adv. 2014, 4, 7703.

3 L. Li, A.G.O. Raji, J.M. Tour, Adv. Mater. 2013, 25. 6298.

4 Y. Liu, X. Zhao, F. Li, D. Xia, Electrochim. Acta 2011, 56, 6448.

5 H. Chen, J. He, C. Zhang, H. He, J. Phys. Chem. C 2007, 111, 18033.

6 S. Lee, J. Ha, H. Cheng, J.W. Lee, T.S. Jang, Y.G. Jung, Y. Huang, J.A. Rogers, U. Paik, Adv. Energy Mater. 2014, 4, 1.

7 B. Sun, Z. Chen, H.S. Kim, H. Ahn, G. Wang, J. Power Sources 2011, 196, 3346.

8 Y. Hou, Y. Cheng, T. Hobson, J Liu, Nano Lett. 2010, 10, 2727.

9 Y. Cao, Z. Wei, J. He, J. Zang, Q. Zhang, M. Zheng, Q. Dong, Energy Environ. Sci. 2012, 5, 9765.

10 C. Wu, X. Wang, B. Ju, X. Zhang, L. Jiang, H. Wu, Int. J. Hydrogen Energy 2012, 37, 14365.

11 F. Cheng, Y. Su, J. Liang, Z. Tao, J. Chen, Chem. Mater. 2009, 22, 898.

12 H.T. Zhu, J. Luo, H.X. Yang, J.K. Liang, G.H. Rao, J.B. Li, Z.M, Du, J. Phys. Chem. C 2008, 112, 17089.

13 H. Wu, X. Wang, X. Wang, X. Zhang, L. Jiang, B. Hu, Y. Wang, J. Solid State Electrochem. 2012, 16, 2941.

14 H. Xia, M.O. Lai, L. Lu, J. Mater. Chem. 2010, 20, 6896.

15 J.G. Wang, Y. Yang, Z.H. Huang, F. Kang, J. Power Sources 2013, 224, 86.

16 C.X. Guo, M. Wang, T. Chen, X.W. Lou, C.M. Li, Adv. Energy Mater. 2011, 1 736.

17 J. Zhang, T. Huang, Z. Liu, A. Yu, Electrochem. Commun. 2013, 29, 17.